

Discovery of Novel Small-Molecule Calcium Sensitizers for Cardiac Troponin C: A Combined Virtual and Experimental Screening Approach

William H. Coldren, Svetlana B. Tikunova, Jonathan P. Davis,[§] and Steffen Lindert^{*,§}



Cite This: *J. Chem. Inf. Model.* 2020, 60, 3648–3661



Read Online

ACCESS |



Metrics & More

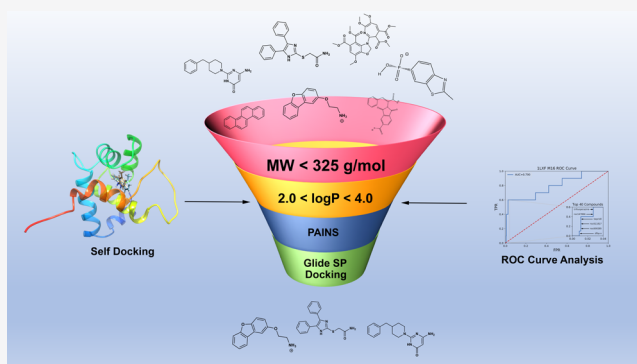


Article Recommendations



Supporting Information

ABSTRACT: Heart failure is a leading cause of death throughout the world and is triggered by a disruption of the cardiac contractile machinery. This machinery is regulated in a calcium-dependent manner by the protein complex troponin. Calcium binds to the N-terminal domain of cardiac troponin C (cNTnC) setting into motion the cascade of events leading to muscle contraction. Because of the severity and prevalence of heart failure, there is a strong need to develop small-molecule therapeutics designed to increase the calcium sensitivity of cardiac troponin in order to treat this devastating condition. Molecules that are able to stabilize an open configuration of cNTnC and additionally facilitate the binding of the cardiac troponin I (cTnI) switch peptide have the potential to enable increased calcium sensitization and strengthened cardiac function. Here, we employed a high throughput virtual screening methodology built upon the ability of computational docking to reproduce known experimental results and to accurately recognize cNTnC conformations conducive to small molecule binding using a receiver operator characteristic curve analysis. This approach combined with concurrent stopped-flow kinetic experimental verification led to the identification of a number of sensitizers, which slowed the calcium off-rate. An initial hit, compound 4, was identified with medium affinity ($84 \pm 30 \mu\text{M}$). Through refinement, a calcium sensitizing agent, compound 5, with an apparent affinity of $1.45 \pm 0.09 \mu\text{M}$ was discovered. This molecule is one of the highest affinity calcium sensitizers known to date.



INTRODUCTION

Heart disease is the leading cause of death in the United States and the world accounting for ~ 23 and $\sim 33\%$ of the total causes of mortality, respectively.^{1,2} Heart failure, in particular, affects approximately 5.7 million people in the United States and was implicated as a contributing cause in one out of every nine deaths that occurred in 2009.³ Heart failure with reduced ejection fraction is a condition where cardiac muscle contraction is too weak to circulate oxygenated blood to the rest of the body upon increased demand (as little increased effort as walking across the room). Therapeutics designed to increase the contractile force of the heart provide a direct avenue to potentially increase quality of life and lower morbidity in people suffering from heart failure. In fact, these compounds are currently used to support patients with severe heart failure until a transplant can occur.⁴

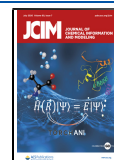
The most populous class of drugs currently on the market that promote cardiac muscle contractility (positive inotropes) operate via the beta-adrenergic pathways and are catecholamines and phosphodiesterase inhibitors.⁵ Examples of these compounds are dobutamine, milrinone, and inamrinone. At the molecular level, these compounds ultimately increase inotropy by increasing the level of systolic Ca^{2+} . Alternatively,

the Ca^{2+} sensitivity of the contractile apparatus could be increased without changing the level of systolic Ca^{2+} as initially hypothesized by Solaro et al.^{6–8} and demonstrated via viral gene delivery to myocardial infarcted mice.⁹ Despite the promise Ca^{2+} sensitization offers in theory and animal models, there is an absence of FDA-approved pharmaceuticals that focus on the modulation of Ca^{2+} sensitivity to treat individuals suffering from chronic heart failure.¹⁰ From 2015 to the present day, out of the 198 novel drugs approved by the FDA, only four of the compounds are designated to treat cardiovascular-related diseases. While heart disease and heart failure in particular remain a significant problem for the world, it is complicated and challenging to bring cardiovascular medications to market.

In order to target Ca^{2+} sensitivity for drug discovery purposes, it is important to understand Ca^{2+} -activated

Received: April 29, 2020

Published: July 7, 2020



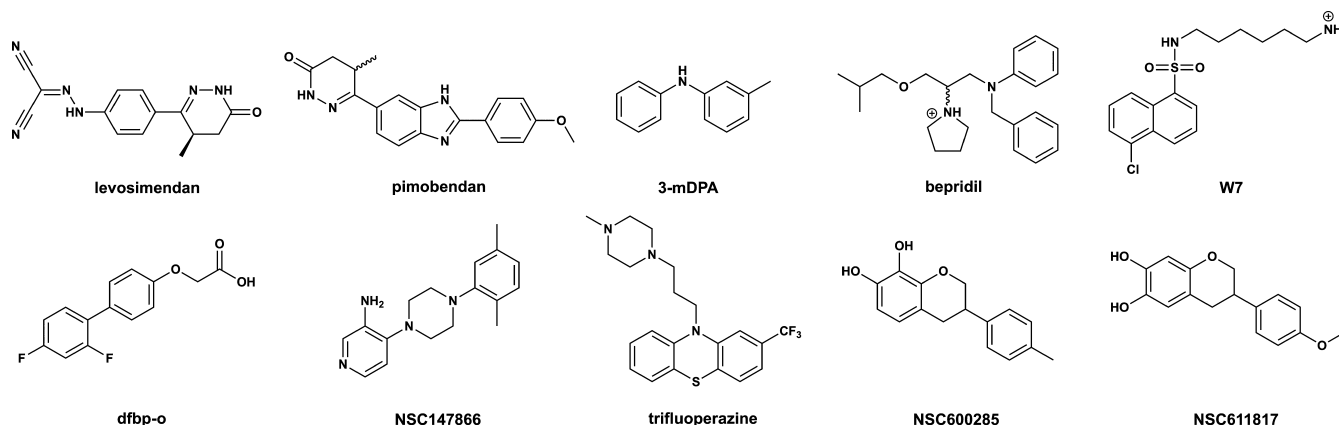


Figure 1. Known cardiac troponin binders and Ca^{2+} sensitivity modulators.

contraction in heart muscle^{11,12} In all nonsmooth muscle,¹³ the three-subunit protein, troponin (Tn), contains a Ca^{2+} -binding subunit (TnC), which triggers the muscle's contractile machinery. Cardiac troponin (cTn) is anchored to the protein tropomyosin by the T subunit (cTnT). The third cTn subunit is known as the inhibitory subunit (cTnI). cTnI contains an approximately 13 residue sequence known as the inhibitory peptide denoted by residues cTnI_{136–149}.^{14–16} cTnI also consists of another region that is essential for enabling muscle contraction, the switch peptide region (cTnI_{150–159}). The inhibitory peptide is named for its primary role in preventing cardiac muscle contraction in the Ca^{2+} -free resting state. cTnI is known to interact with all components of the thin filament.¹⁷ When the cTnI switch peptide (cTnI_{150–159})¹⁶ strongly associates with the N-terminal domain of cTnC (cNTnC) in a Ca^{2+} -dependent fashion, cTnI releases its hold on actin giving tropomyosin the freedom to “rock and roll,” freeing myosin binding sites on actin, allowing for thin and thick filament cross-bridges to form and ultimately resulting in heart muscle contraction.¹⁸

The cardiac Ca^{2+} -binding domain, cTnC, is of key importance in this study as it is a prime target for small molecule therapeutics. It is the N-terminal domain, cNTnC, which through Ca^{2+} -mediated action can strongly interact with the switch peptide region of cTnI when a hydrophobic patch is exposed.¹⁹ Long-timescale molecular dynamics (MD) simulations have shown that Ca^{2+} bound cNTnC samples a semi-open configuration much more frequently than apo cNTnC and the relative free energy costs for hydrophobic patch opening are ~ 8 and ~ 20 kcal/mol, respectively.^{20–23} Additionally, umbrella sampling simulations have suggested that mutations and ligand binding significantly impact the energetics of patch opening.^{24,25} Experimentally, small molecule binding to the hydrophobic patch has been shown to have Ca^{2+} modulation properties.^{6,26–30} The total number of known Ca^{2+} sensitivity modulating compounds is somewhat limited. Some of the best known Ca^{2+} -sensitizing compounds are shown in Figure 1. Three of these compounds are prescribed to treat heart failure outside of the United States: bepridil, levosimendan, and pimobendan. Levosimendan did not reach FDA approval, and the prescription of bepridil was discontinued because of the propensity of these compounds to cause fatal cardiac arrhythmias, notably the polymorphic ventricular arrhythmia torsade de pointes (literally twisting of the peaks). Increasing the affinity and sensitivity of cNTnC for Ca^{2+} could lead to increased contractility in the heart. On a

fundamental level, the discovery of additional novel small molecule sensitizers is one important avenue in the heart failure drug discovery field as it will hopefully help to highlight key structural motifs of effective sensitizers. Additional studies to find links between the structure and activity could help refine our understanding of important protein–ligand interactions and help guide the rational design and optimization of potential therapeutics.

Previous computational and experimental studies have shown that small molecules with affinity for the hydrophobic patch can lead to increased protein Ca^{2+} sensitivity.^{26,30–36} Recently, we combined a high-throughput virtual screening approach, receiver operator characteristic (ROC) curve analysis, as well as experimental verification assays including steady-state fluorescence and stopped-flow kinetics to identify two novel cNTnC Ca^{2+} sensitizing agents.³⁷ The work described in this article extends upon this proof of principle study. We have increased the number of docking methodologies tested as well as the number of protein receptors, some from Gaussian-accelerated molecular dynamics (GaMD), used in our relaxed complex scheme (this scheme accounts for the flexible nature of both the receptor and the small molecule).^{38–40} Importantly, we used a self-docking workflow in order to evaluate each docking methodology and its ability to accurately reproduce bound poses of ligands in experimentally determined cNTnC–ligand complexes before proceeding to active/decoy docking and ROC curve analysis. We investigated new, curated libraries of drug-like small molecules containing more diverse sets of pharmacophores and functionality and utilized a cheminformatics approach to prefilter these compounds and streamline docking. This new procedure led to an increased number of positive hits for small molecule Ca^{2+} sensitizers. Hits discovered by our virtual screening process were tested *in vitro* by stopped-flow kinetics in order to measure the calcium off-rate. Additionally, compounds that initially performed well in stopped-flow kinetic screenings were further characterized with dose response curves. Ultimately, upon iterative refinement, we discovered a small molecule with a binding constant sixfold lower than the best currently known Ca^{2+} sensitizers.⁴¹

■ MATERIALS AND METHODS

Protein Selection and Preparation. We performed a search for human cNTnC experimental structures archived in the RCSB protein data bank. We selected receptor conformers that were in complex with Ca^{2+} sensitivity modulators in order

to compare our theoretical docking to experiment. PDBs selected were: 5WCL, 5W88, 2L1R, 2KRD, 2KFX, 1LXF, and 6MV3. 5WCL and 5W88 contain 3-methyl-*N*-phenylaniline (3-mDPA) in two different modes; one (“solvent exposed mode”) in which the methyl group of the ligand is directed toward a more solvent-exposed region of the protein (Met60 and Val64) and the other (“peptide mode”) where the methyl group associates more closely to the cNTnC–cTnI interface.³³ Both 5WCL and 5W88 are structures of a cardiac troponin chimera, in which the switch peptide region of cTnI is tethered to the N-terminal regulatory domain. PDB IDs 2KRD, 2KFX, and 6MV3 are all bound to the compound W7; however, the nature of the protein complex differs in each case. 2KRD contains cNTnC along with the switch peptide and the ligand while 2KFX is simply cNTnC and the ligand.^{42,43} 6MV3 is the most recent PDB of all those listed above and is again the chimeric version of cNTnC tethered to the switch peptide region of cTnI.⁴⁴ 2L1R contains cNTnC in complex with the switch peptide and the Ca²⁺ sensitizer 2-((2',4'-difluoro-[1,1'-biphenyl]-4-yl)oxy)acetic acid (dfbp-o). Finally, 1LXF is a structure of cNTnC in complex with the switch peptide and the Ca²⁺ sensitizer bepridil.⁴⁵ All selected proteins were derived from NMR experiments and contained multiple solved conformers. Each conformer was extracted yielding a total of 176 structures that we used in our docking studies.

In order to account for troponin conformational flexibility not represented in the protein data bank, additional protein receptor conformations were obtained from 300 ns GaMD production simulations performed with Amber18 and the Amber14ffSB forcefield.^{46–48} We simulated the representative conformers of proteins 1LXF, 2KRD, and 1MXL. 1MXL, not listed above, is an NMR structure of cNTnC in complex with cTnI_{147–163}, but does not have any ligand bound.⁴⁹

The final structures to be used for docking studies were obtained by clustering each 300 ns GaMD simulation individually. The simulations were clustered to obtain 10 most representative frames of the trajectory based on an agglomerative hierarchical algorithm as implemented by AMBER's CPPTRAJ. The centroid of each cluster was extracted for further use in active/decoy docking studies. This procedure yielded an additional 30 conformers for the docking analysis. For a much more detailed description of the MD procedure, please refer to the [Supporting Information](#).

Finally, all 206 conformers were imported into Schrödinger's Maestro and prepared using Schrödinger's Protein Preparation Wizard.⁵⁰ The C-terminus of cNTnC was capped by the addition of an *N*-methyl amide in lieu of a carboxylate moiety.⁵¹ The protonation states of all titratable residues were assigned using EPIK with a pH constraint of 7.0 ± 1.0.⁵²

Ligand Preparation. The LigPrep module of the Schrödinger Suite was used to prepare each ligand for docking. All protomers, tautomers, and stereoisomers were generated for each input. Potential protonation states were assigned by EPIK for a pH value of 7.0 ± 1.0.^{52,53} The only exception to this was the known sensitizer levosimendan where the enantiomeric center is known to be (*R*) in the active form.⁵⁴ The coordinates of bepridil (1LXF), dfbp-o (2L1R), 3-mDPA (5W88 and 5WCL), and W7 (2KFX, 2KRD, and 6MV3) were extracted from their corresponding PDBs while known actives levosimendan, pimobendan, trifluoperazine, NSC611817, NSC600285, and NSC147866 were built using Schrödinger's Maestro. All other structures used in our docking protocol

came from existing SDF files containing 3-dimensional coordinates.

Self-Docking Methodology. We docked extracted ligands from PDB IDs 1LXF, 2L1R, 2KFX, 2KRD, 6MV3, 5WCL, and 5W88 back into their respective receptor conformations in order to determine which docking program, scoring function, and adjustable parameters performed best in terms of reproducing experimentally bound poses in cTnI. This was assessed by the calculation of in-place root-mean-square deviation (rmsd) (described below) of the top scoring docked pose to the experimental position. Docking was carried out on the representative NMR conformer for each of the seven PDBs listed above. Our cutoff criterion for success was an in-place rmsd value of 2.00 Å or lower. We tested the following docking algorithms: AutoDock Vina, Glide HTVS, Glide SP, and Glide XP.

The main differences between AutoDock Vina and Glide are due to the scoring function and search algorithm. AutoDock Vina employs both knowledge-based and empirical scoring terms (based on the X-score function), treats nonpolar hydrogens implicitly, and neglects the direct treatment of electrostatics.^{55–57} Schrödinger's Glide HTVS and SP use the same empirical-based scoring function while Glide XP imposes harsher penalties to poses that violate physical chemistry-based criteria such as not positioning charged and polar groups toward solvent exposed areas.^{58,59} Glide uses a series of hierarchical filters to locate candidate poses and notably performs a forcefield-based geometry refinement for final pose selection. Glide's search is deterministic in nature while AutoDock Vina uses a stochastic global optimization and gradient descent (with respect to the scoring function).^{55,58}

For AutoDock Vina, it was necessary to further adjust our prepared proteins and ligands to be compatible for docking.⁵⁵ AutoDock tools was used to merge all nonpolar hydrogens into their neighboring carbons for both the protein receptor conformations and their ligands. Two separate search spaces were defined, one as a 20 × 20 × 20 Å³ box and the other was a 50 × 50 × 50 Å³ box positioned at the experimental ligand's center of mass. We tested exhaustiveness levels of 8, 20, and 200 for each box size. Increasing the exhaustiveness parameter within AutoDock Vina expands the iterations spent searching ligand–protein interactions in order to increase the chance of finding a global minimum with respect to the scoring function. In each case, the ligand was allowed to be flexible while the receptor conformation remained rigid.

The three core methods of Schrödinger's Glide (HTVS, SP, and XP) were tested with their default values as implemented in the Schrödinger 2018-3 release as well as with adjustments to customizable parameters (enhanced sampling during predocking conformer generation and expanded sampling for the selection of initial docked poses to further refinement).^{58–60} Before docking, it was necessary to generate a receptor grid or search space for use with Glide's docking methods.

In general, receptor grids for Glide simulations were generated by selecting the ligand within Maestro's workspace where it set the search area on the center of the ligand and allowed the centroids of any docked species to fully explore a 10 × 10 × 10 Å³ inner search space, while the periphery of the ligand was able to extend out to 20 × 20 × 20 Å³. The OPLS3e forcefield was selected in each case to generate the desired search grid.⁶¹ In addition, all hydroxyl groups were selected to be freely rotatable in the search area. Ligand sampling was set

as flexible in all cases allowing for inversions at pyramidal nitrogen centers as well as different available ring conformers where appropriate. Nonplanar amide configurations were penalized in all cases.

For the docking runs, Glide's HTVS methodology was used exclusively without adjustments. In the first trial, Glide SP was used with default values, and in the second (referred to as SP2), enhanced sampling was used for ligand conformer generation and expanded sampling for the selection of initial docked poses. Glide XP was also initially used without adjustments (enhanced sampling is a nonadjustable parameter, *i.e.*, on by default in this case), and in the second trial (referred to as XP2), expanded sampling was enabled for the selection of initial docked poses.^{58–60}

In-place rmsds were calculated for the five combinations of methods and parameters. These rmsds were calculated by the comparison of all heavy atoms and polar hydrogens of the docked molecule to the experimental coordinates without superposition. Nonpolar hydrogens were omitted from the calculation. For AutoDock Vina and Schrödinger's Glide, an in-house python script was written in order to calculate the rmsds. Additionally, Glide's automatic rmsd calculation was implemented in order to cross-check docked compounds.

Active/Decoy Screening and ROC Curve Analysis. Optimized parameters found for AutoDock Vina and Schrödinger's Glide SP performed equally well during the self-docking phase in terms of reproducing the known bound poses for the NMR conformers. In order to break this tie and select a docking method to use for the virtual screens, the representative conformers from PDB IDs 1LXF, 2L1R, 2KFX, 2KRD, 6MV3, 5WCL, and 5W88 were used in trial active/decoy screenings to select which docking method had the best capacity to distinguish between known active compounds.

A set of small molecules curated as decoy ligands were obtained from Schrödinger. This set contained 1000 ligands with an average molecular weight (MW) of 360 g/mol^{58,60} (close to the 298 g/mol average of the ten known actives). The active compounds docked against the assumed decoys are shown in Figure 1. The ten compounds expanded to 19 total isomers/protomers post-LigPrep.

All 1019 ligand structures were docked into each of the seven PDB structures listed above using Glide SP with default options and then again with AutoDock Vina using a 50 × 50 × 50 Å³ box size and an exhaustiveness of 20. The resulting docked poses were ranked by their docking score. The top scoring pose of each protomer/stereoisomer was kept. The true positive rates (TPRs) and false positive rates (FPRs) were calculated at each threshold in order to produce ROC curves. The area under each ROC curve was calculated using Python's scikit-learn library (ver. 0.22.1).⁶² In addition, enrichment factors were calculated for each receptor conformation according to the following equation.

$$\begin{aligned} \text{EF} &= \frac{N_{\text{active in top 40}}}{40} \times \frac{N_{\text{total}}}{N_{\text{active}}} = \frac{N_{\text{active in top 40}}}{40} \times \frac{1010}{10} \\ &= 2.525 \times N_{\text{active in top 40}} \end{aligned}$$

Note, the values for N_{total} and N_{active} were 1010 and 10, respectively, instead of 1019 and 19. If the LigPrep procedure for an active compound produced more than one output structure (two structures for bepridil, enantiomers of one another, *e.g.*), the top scoring structure was kept and lower scoring structures discarded making the assumption that the

potent form would be the one with better binding affinity. In order to set a reasonable threshold for number of compounds to purchase and test, a cutoff of 40 compounds was selected for calculating enrichment factors for each receptor conformation. In the perfect limiting case all ten, known active compounds would be scored with better affinities than all 1000 decoy compounds, the AUC would be 1.00, and the enrichment factor would be 25.25.

Based on the results of these initial active/decoy screens, Glide SP with default parameters was selected as our preferred docking method for the blind screening. Using Glide SP with default parameters, we tested the remainder of the 206 receptor conformations in active/decoy screenings following the exact procedure listed above. After completing active/decoy screenings in all 206 receptor conformations, the three receptors with the highest enrichment factors and subsequently highest AUCs (in the case of enrichment factor tie) were selected for blind screening and consensus docking.

Small Molecule Library Selection and Blind Screening. We selected the ChemBridge EXPRESS-Pick Collection for screening in this study, which contained 504,599 small drug-like molecules. In order to increase the efficiency of our screening process, we prefiltered compounds based on MW, predicted solubility, and excluded compounds with functional groups implicated as pan-assay interference compounds.⁶³ This prescreen was performed using the 2019.03 release of RDKit package implemented through Python 3.6.⁶⁴ The SDF file containing all 504,599 compounds was used to convert each ligand into an RDKit molecule object. Molecule objects contained all of the necessary descriptors of the molecule (atomic identity, position, connectivity, *etc.*) in order to perform further calculations. In order to increase the computational tractability of screening a large database using the Glide SP model, all compounds with MWs above 325 g/mol were filtered out to maintain sizes closer to the average of known actives, ~300 g/mol. PAINS filters A, B, and C as implemented in RDKit were utilized to remove compounds in these families, as described by Baell and Holloway.⁶³ Molecules with predicted logP values under 2.0 and over 4.0 were discarded. These logP parameters were calculated from the molecule objects using Wildman and Crippen's model.⁶⁵ With all of these filters in place, the original 504,599 molecules in the ChemBridge EXPRESS-Pick Collection were reduced to 90,759. The initial MW filter removed the majority of compounds (328,353) while the second phase logP filter removed an additional 80,668 leaving 95,478 compounds. The final PAINS filter removed 4719 compounds leaving 90,759. These 90,759 remaining compounds were prepared with the Schrödinger LigPrep module leading to a final number of 135,247 stereoisomers/protomers used for screening.

These final 135,247 structures were all docked using Glide SP with default values into the three most predictive receptor conformations as determined by our active/decoy ROC curve analysis. The ranking of the docked molecules was averaged across the three separate docking simulations and used to select a top set of promising compounds to test experimentally. A final filter was utilized on docked compounds, the Virtual Computational Chemistry Laboratory Web Service's ALOGPS 2.1 lipophilicity predictor. This program has been shown to provide logP and logS values closer to experimental values than Crippen's model. Because of server limitations this was only used on a final, docked set of the top 50 candidates and not implemented in the prescreen phase. An upper logP cutoff

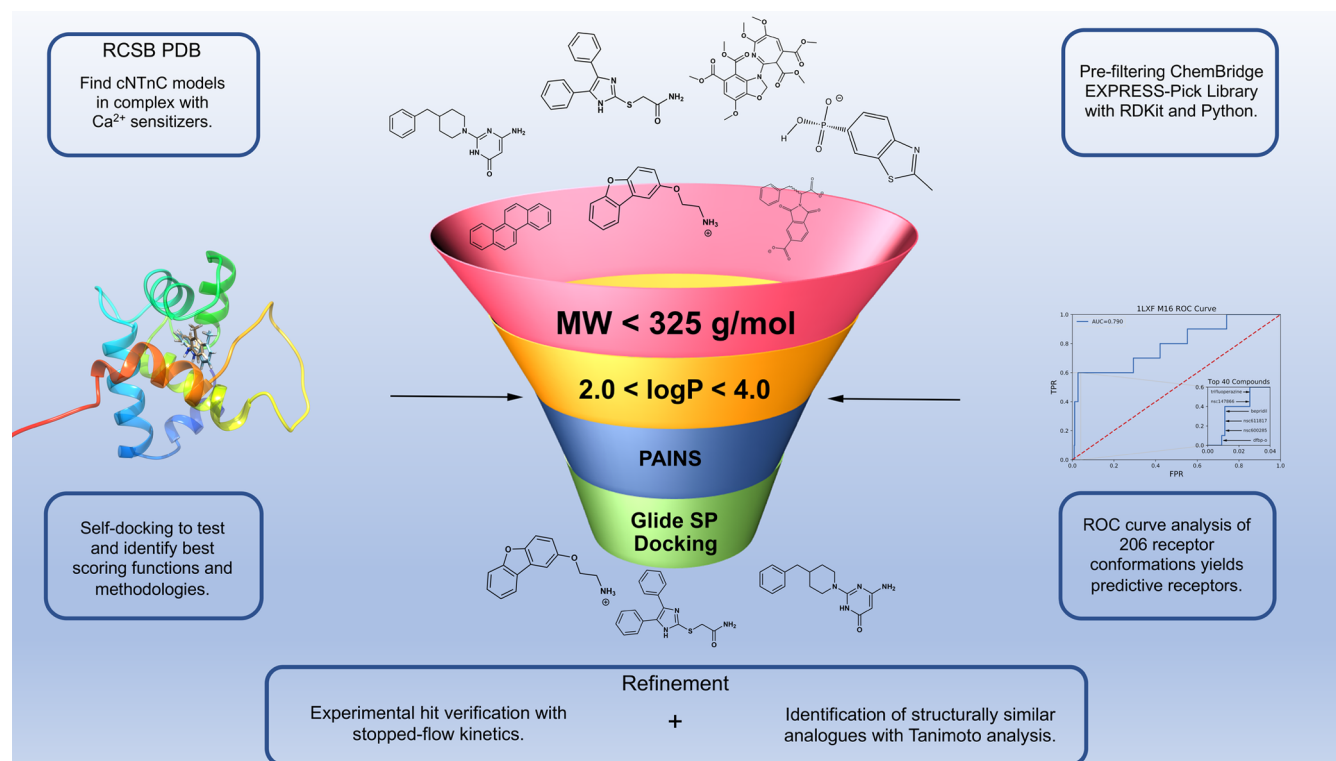


Figure 2. Drug discovery workflow.

of 3.6 was used in this case based on solubility data from our prior experimental screening (work unpublished). After filtering by these criteria, the poses of the top docked compounds were visually inspected. After visual confirmation of binding in the hydrophobic patch, 40 compounds were ordered directly from ChemBridge and tested *in vitro*.

Preparation of Proteins for Biochemical Studies. The T53C-IAANS chimera (herein designated as chimera) was generated as previously described.¹⁹ Briefly, a Pet17b vector containing the chimera was transformed into Rosetta 2 (DE3) competent cells and expressed after induction with 1 mM IPTG. The cells were resuspended in buffer A (20 mM Tris, 2 mM ethylenediaminetetraacetic acid, 6 M urea, 0.5 mM dithiothreitol, at pH 8.0) containing a protease inhibitor cocktail. The cells were sonicated on ice and the resulting solution was centrifuged at 19,000 rpm at 4 °C for 30 min and the supernatant was collected. Ammonium sulfate was added at 20% saturation to remove some of the contaminating proteins. The solution was centrifuged again at 19,000 rpm at 4 °C for 30 min and the supernatant was collected. Ammonium sulfate was then added to 60% saturation to precipitate the chimera. The solution was centrifuged at 19,000 rpm at 4 °C for 30 min and the pellet was collected. The pellet was resuspended in 30 mL buffer A and dialyzed at least four times against 1 L of the same buffer. The solution was then loaded onto an (diethylamino)ethyl-sepharose column equilibrated with buffer A. After an initial wash with buffer A, a 500 min gradient was applied with 0–100% of buffer B (buffer A containing 0.3 M NaCl). Fractions containing chimera were collected and further purified using 50 kDa cut-off Amicon Ultra-15 Centrifugal Filter Units. Flow-through samples containing the chimera were collected and dialyzed against 4 L of 10 mM MOPS, 150 mM KCl, at pH 7.0 at least four times. The

purified chimera was labeled with the environmentally sensitive fluorescent probe IAANS as previously described.⁶⁶

Stopped-Flow Fluorescence Measurements. All kinetics measurements were carried out at 15 °C using an Applied Photophysics Ltd. (Leatherhead, UK) model SX.18MV stopped-flow apparatus with a dead time of ~1.4 ms. IAANS fluorescence was excited at 330 nm with emission monitored using a 420–470 nm band-pass interference filter (Oriel, Stratford, CT). 10 mM EGTA in stopped-flow buffer (10 mM MOPS, 150 mM KCl, at pH 7.0) in the absence or presence of compounds was used to remove Ca²⁺ (200 μM) from T53C-IAANS chimera (0.5 μM) in the absence or presence of compounds also in the stopped-flow buffer. Varying concentrations of each compound were individually added to both stopped-flow reactants. Data traces were fit using a program (by P.J. King, Applied Photophysics Ltd.) that utilizes the nonlinear Levenberg–Marquardt algorithm. Each k_{off} represents an average of at least three separate experiments ± standard error, each averaging at least five shots fit with a single exponential equation.

Identification of Compounds Highly Similar to Top Experimental Hit. The top performing Ca²⁺ sensitizer identified in the first round of stopped-flow kinetics was compared to all 504,599 compounds in the unfiltered ChemBridge EXPRESS-Pick Collection in order to determine highly similar analogues for a second round of experimental tests.

The RDkit library for python 3.6 was used in order to perform molecular fingerprinting on all 504,599 compounds (MW filters as well as log *P* filters were removed at this stage, PAINS filtering was performed on the final set of molecules to assure no problematic functional groups were present). The Tanimoto similarity coefficients between the lead experimental compound and the entire Express library were calculated. The

RDkit-specific molecular fingerprinting algorithm was used (a full description of this scheme is discussed in the RDKit Book.⁶⁴ Using a Tanimoto coefficient cutoff of 0.7, nineteen additional molecules were filtered and docked into the top performing conformer, 1LXF M16, using optimal Glide SP parameters. Five small molecules were selected for a second round of experimental testing based upon inspection three key criteria: visualization of the 2D structures to confirm their similarity to the initial hit using chemical intuition, visualization of the docked poses to assure they were correctly located within the hydrophobic patch, and assessment of the docking scores in order to select those that ranked best.

The refined hit obtained from our similarity search and the second round of experimental assays was again compared to all 504,599 ChemBridge EXPRESS-Pick Collection compounds and similarities were calculated. This time, compounds with Tanimoto coefficients over 0.55 were selected, previously purchased compounds removed, and the remaining 42 compounds redocked into the top conformer, 1LXF M16. After this, two approaches were taken. The average docking score among all 42 compounds was used as a filter (compounds scoring worse than the average were thrown out). After application of the scoring filter, the remaining compounds were sorted from highest to lowest similarity to the newest hit, filtered for PAINS functionality, and the top ten were selected. The second approach disregarded docking score and only selected the top ten most similar compounds. The top ten compounds from each filtering method listed above (giving a final total of twenty compounds) were visually inspected as described above and from those, five final compounds were purchased for experimental testing based on their uniqueness and structural differences from previously screened, poor performing compounds.

RESULTS AND DISCUSSION

We utilized a computer-aided drug discovery approach in order to identify high affinity, novel Ca²⁺ sensitizing compounds targeting the N-terminal, regulatory domain of human cardiac troponin. Expanding upon our previous study that used computer-aided drug discovery targeting cNTnC,³⁷ here we have refined our methodology to account for different docking algorithm's ability to reproduce experimentally bound poses of known active compounds. We screened more compounds with a strong focus on drug-likeness and solubility. In addition, we expanded the number of tested protein receptor conformers from 35 to 206 in order to increase the chances of finding a conformer with the best possible ability to identify known active compounds by ROC curve and enrichment factor analysis. A summary of our drug discovery workflow can be found in Figure 2.

Self-Docking rmsd Comparisons. We hypothesized that docking algorithms that accurately reproduced binding poses of known cNTnC binders would likely predict binding poses of unknown compounds best. We tested Glide scoring functions HTVS, SP, SP2, XP, and XP2 as well as AutoDock Vina using two different box sizes and three different levels of exhaustiveness for their ability to dock known cNTnC binders correctly. The representative conformer of small molecule containing PDB IDs 1LXF, 2KRD, 2KFX, 6MV3, 2L1R, 5WCL, and 5W88 had their coordinating ligand removed and redocked with each methodology listed in the [Materials and Methods](#) section above. In-place rmsds were calculated to evaluate relative docking algorithm performance. The set of

AutoDock Vina parameters that produced the lowest rmsd results (averaged across each protein) were a box size of 50 × 50 × 50 Å³ and an exhaustiveness of 8 (Table 1). The small

Table 1. Self-Docking rmsd (Å) Comparison for the Representative Conformers of Each PDB

docking algorithm	1LXF	6MV3	2KFX	2KRD	2L1R	5W88	5WCL
Vina Box: 20 ³ Å ³ Ex: 8	5.41	3.23	1.59	2.99	0.46	1.40	4.95
Vina Box: 20 ³ Å ³ Ex: 20	5.36	3.26	1.88	3.47	0.44	1.40	4.95
Vina Box: 20 ³ Å ³ Ex: 200	5.37	3.22	1.84	3.39	0.42	1.40	4.94
Vina Box: 50 ³ Å ³ Ex: 8	4.76	2.10	1.37	2.02	0.80	1.38	4.91
Vina Box: 50 ³ Å ³ Ex: 20	5.99	3.46	1.62	2.20	0.39	1.41	12.1
Vina Box: 50 ³ Å ³ Ex: 200	3.55	3.16	1.77	2.84	0.43	1.36	4.95
Glide HTVS	N/A	2.91	4.02	4.64	1.94	1.21	5.77
Glide SP1	4.26	1.49	3.86	5.02	1.72	1.62	5.68
Glide SP2	5.96	3.02	4.10	5.15	1.96	2.31	5.68
Glide XP1	2.54	5.75	4.43	4.77	2.43	2.31	5.80
Glide XP2	6.52	4.86	4.03	5.62	1.72	2.29	5.64

molecules associated with PDB IDs 2KFX, 2L1R, and 5W88 (W7, dfbp-o, and 3-mDPA) had top scoring poses identified with rmsds of 1.368, 0.798, and 1.377 Å, respectively. We did not observe qualitatively different results between the six different parameter sets selected for AutoDock Vina. In every case, ligands from 2KFX, 2L1R, and 5W88 were classified as hits under our 2.0 Å rmsd cutoff criteria.

Using Schrödinger's Glide functionality with the HTVS, SP, and XP scoring functions as well as parameter modifications in protocols SP2 and XP2 yielded zero to three correctly identified poses. The number of hit results for HTVS, SP, SP2, XP, and XP2 were two, three, one, zero, and one, respectively (Table 1). Glide SP with default parameters yielded a three out of seven-hit result (similar to AutoDock Vina) with the best performing score function and parameters. The representative receptor conformer for PDB IDs 6MV3, 2L1R, and 5W88 with corresponding small molecules W7, dfbp-o, and 3-mDPA had top scoring poses with rmsds of 1.487, 1.715, and 1.615, respectively (Figure 3). A comparison of all rmsds for AutoDock Vina and Glide can be found in Table 1. Glide HTVS was unable to locate a docked pose of bepridil in the representative model of 1LXF because of HTVS's reduced sampling (a trade-off to increase the speed of docking per compound). The lack of result is denoted in Table 1 by "N/A".

PDB receptors 2L1R and 5W88 remained consistent as hits among AutoDock Vina and Glide SP. These structures are cNTnC in a noncovalent complex with the switch peptide region, cNTN₁₄₇₋₁₆₃ in the case of 2L1R and cNTnC tethered to the switch peptide in the chimeric 5W88. Additionally, Vina correctly identified the bound pose of W7 for 2KFX, a structure of cTnC not in complex with the switch peptide, whereas Glide SP succeeded in docking W7 for the 6MV3 chimera, in which cNTnC is tethered to the switch peptide.

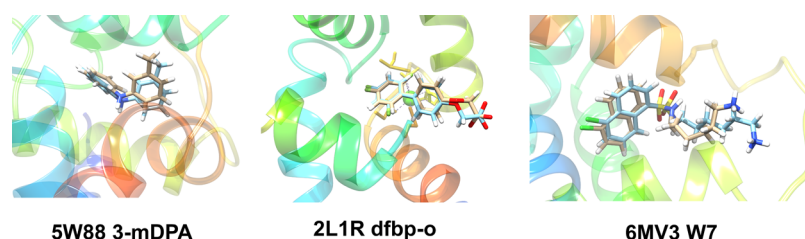


Figure 3. Protein receptors with an experimental pose (beige) and docked ligand (cyan) of top performing Glide SP self-docking simulations. rmsds of 3-mDPA, dfbp-o, and W7 are 1.49, 1.72, and 1.62 Å, respectively.

Although results from AutoDock Vina are stochastic in nature, the scoring function remained the same in all of the Vina docking simulations. Because of a consistent scoring function (a modified version of Xscore),⁵⁵ even if the exhaustiveness and/or the search area were increased, well-bound and well-scored poses should remain the same (unless there was a secondary binding site). Thus, qualitatively, we did not observe much variance of in-place rmsd for different Vina parameter sets.

The scoring functions for Glide HTVS and SP are identical while XP employs a more complex scheme. Glide docking simulations are deterministic in contrast to AutoDock Vina. Interestingly, despite enhanced conformational sampling and a more sophisticated scoring function in Glide XP, for our particular protein system Glide SP performed the best among all investigated Glide docking algorithms (Table 1).

In general, regardless of docking algorithm, the representative protein receptor conformations for 1LXF, 2KRd, and 5WCL did not perform well in self-docking trials. 5WCL is a secondary structure for the 3-mDPA bound protein. 5W88 and 5WCL capture two significant small molecule orientations found as contributors during the NMR studies of cNTnC–3-mDPA. In one case, the methyl group located on the phenyl ring of the small molecule was oriented toward the interior of the hydrophobic patch (this conformer was deposited as 5W88, known as peptide mode). In the other case, the methyl group was directed outside of the hydrophobic patch toward the solvent (deposited as 5WCL, known as solvent exposed mode). From a molecular simulation standpoint, it is unsurprising that the solvent exposed pose for 5WCL could not be easily recovered by docking because of the relative penalization that the methyl group received by not maximizing nonbonded interactions. When self-docking 3-mDPA into 5WCL, both AutoDock Vina and Glide SP favored poses where the methyl group was not “solvent exposed”.

It is possible that protein receptor conformations for 1LXF and 2KRd performed poorly during self-docking trials because of the large amount of degrees of freedom in the respective small molecule ligands and subsequently their size as well. Using a methodology that allows for flexibility in the protein receptor could help alleviate inherent unfavorable clashes as determined by the current docking protocols’ scoring functions.

Both Glide SP and AutoDock Vina performed equally well during the self-docking trials. Each was able to reproduce three known docked poses of their corresponding small molecules. We hypothesized that identifying a scoring function and docking algorithm that predicted accurate poses with better scores would enable our blind studies to discover more potent potential hints. In order to down-select to one docking algorithm used in the blind screens, the results of active/decoy

screenings were taken into account in order to break this self-docking rmsd tie.

Optimal Parameter Active/Decoy Comparisons. By docking the known active compounds along with a set of 1000 compounds assumed to be inactive decoys into the seven representative conformers for PDB IDS 1LXF, 2L1R, 2KFX, 2KRd, 6MV3, 5WCL, and 5W88 the predictivity of the Glide SP and AutoDock Vina docking algorithms was assessed by ROC curve analysis. The most desirable outcome would be for active compounds to have a more negative docking score (indicating higher predicted binding affinity) than all of the decoy compounds. The ROC area under the curve (AUC) assesses preferential scoring of actives *versus* decoys for all docked compounds as a whole while the enrichment factor measures preferential scoring of actives *versus* decoys within the top 40 compounds. All resulting enrichment factors and AUC values are displayed in Table S1. For each NMR conformer except for 5W88, Glide SP was more predictive as determined by the enrichment factor (where ties were broken with AUC).

For the purposes of this study, a higher enrichment factor was given more weight than the AUC for each ROC curve. Early enrichment is beneficial when planning to order a limited number of compounds (in this case 40). A software and protein receptor that allows for rapid identification of known active compounds makes it statistically more likely that a selection of 40 compounds from blind screening will contain an active compound. Thus, for our cardiac troponin/Ca²⁺ sensitizer system the most accurate and predictive methodology was determined to be Glide SP. All subsequent dockings were performed with Schrödinger’s Glide SP.

Glide SP Top Performing Receptor Conformations. Having established that the Glide SP docking methodology was the most predictive for our system of interest, we set out to evaluate a larger number of protein receptor conformers in order to identify the three most highly predictive conformers in terms of enrichment factor and area under their respective ROC curves. 206 receptor conformers were compiled from two main sources: NMR structures of cNTnC in complex with known Ca²⁺ modulators and representative structures obtained from GaMD simulations of a subset of these structures. All downloaded PDB structures (5WCL, 5W88, 2L1R, 2KRd, 2KFX, 1LXF, 1MXL, and 6MV3) were derived from NMR measurements and each deposited PDB contained the coordinates for several different NMR conformers yielding a total of 176 receptor conformers (a summary of these conformer models per PDB can be found in Table S2). In addition, the representative models from 1LXF, 2KRd, and 1MXL were subjected to 300 ns GaMD simulations. The rationale for using 1LXF and 2KRd for GaMD simulations was that these contained the two largest ligands, bepridil and W7

and would hopefully maintain the largest opening of the hydrophobic patch for docking. 1MXL was selected in addition to 1LXF and 2KRD for contrast as it contained no ligand. The coordinates for each protein were clustered to obtain ten representative receptor conformers for each of the three simulations giving a total of 30 extra receptor conformers and an overall total of 206 receptor conformers when added to those taken directly from the PDBs listed above.

The ten known active compounds from literature were subjected to Schrödinger's LigPrep utility to account for appropriate potential protomers/stereoisomers resulting in 19 final structures. These 19 prepped structures along with the set of 1000 already LigPrepped decoys were combined for a total of 1019 compounds. Each of these 1019 compounds was docked into each of the 206 receptor conformers listed above using the Glide SP docking algorithm determined to be the most predictive at identifying known sensitizers and reproducing their docked poses fairly well. For each of the docking simulations the poses were ranked by docking score. The top scoring protomer/stereoisomer of the 19 active compounds was retained and the others removed. This prevented duplicates during our ROC curve and enrichment factor analysis (the theoretical maximum number of compounds was 1010). All docking simulations into the 206 receptor conformers were ranked by enrichment factor and subsequently AUC in order to break ties (see Table 2 for the

The highest AUC representing perfect predictivity would arise if the top ten scoring compounds were all known actives and all decoys had been scored worse; this would correspond to an AUC of 1.00.

All of the top scoring conformers (those able to discriminate four known actives or more within the top 40 ranked compounds) came from different structural conformers provided by the NMR structure of bepridil-bound 1LXF. The only exception to this was the eighth most predictive conformer, which came from the W7-bound 2KRD NMR structure. The top three scoring models were NMR conformers 1LXF M16, 1LXF M28, and 1LXF M6. These models provided enrichment factors of 15.2 (six known active compounds in the top 40), 10.1 (four known active compounds in the top 40), and 10.1, respectively. The AUCs for these three top models were 0.79, 0.86, and 0.84, respectively. The eighth-highest ranked receptor conformer was 2KRD M17 with an enrichment factor of 10.1 and an AUC of 0.73. Example ROC curves are shown in Figure 4.

It is noted that the conformers for 2KFX did not contain the switch peptide. These conformers performed rather poorly in terms of known active identification with the maximum enrichment factor being 5.0 (see Table S3), suggesting that compound-switch-peptide interactions are a crucial contributor to ligand binding. The majority of 2KFX conformers only have an enrichment factor of 2.5 (corresponding to one known active identified in the top 40). Bepridil is the largest in terms of volumetric size of the small molecules.²⁵ It stands to reason that even though the self-docking rmsd of bepridil in 1LXF was rather poor, the cavity of 1LXF is enlarged relative to the other PDB conformers. This could enable other small molecules the flexibility to orient themselves in a fashion that maximizes their potential docking score relative to the decoy structures.

Given the results outlined above, we selected the two most predictive receptor conformers (1LXF M16 and 1LXF M28) for our blind virtual screening. Additionally, in order to diversify our blind screening receptor models, we also selected conformer 2KRD M17 for our final docking simulations. While receptor conformer 2KRD M17 would not technically rank third amongst all of the conformers, the enrichment factor of 10.1 matched the rest of the top scoring conformers and the AUC was only slightly lower (Table 2).

Blind Screening Results. We docked 135,247 LigPrepped structures from the ChemBridge EXPRESS-Pick Collection into the three predictive receptor conformers (1LXF M16, 1LXF M28, and 2KRD M17) using the Glide SP docking

Table 2. Top 10 Most Predictive cNTnC Conformers Resulting from Active/Decoy Screens

receptor conformer	enrichment factors	AUCs
1LXF_M16	15.2	0.79
1LXF_M28	10.1	0.86
1LXF_M6	10.1	0.84
1LXF_M22	10.1	0.80
1LXF_M2	10.1	0.80
1LXF_M21	10.1	0.79
1LXF_M15	10.1	0.75
2KRD_M17	10.1	0.73
1LXF_M14	7.6	0.81
1LXF_M8	7.6	0.80

top 10 conformer results; all results available in Table S3). The theoretical maximum enrichment factor would occur if all ten known active compounds were ranked in the top 40 (out of 1010 total), corresponding to an enrichment factor of 25.25.

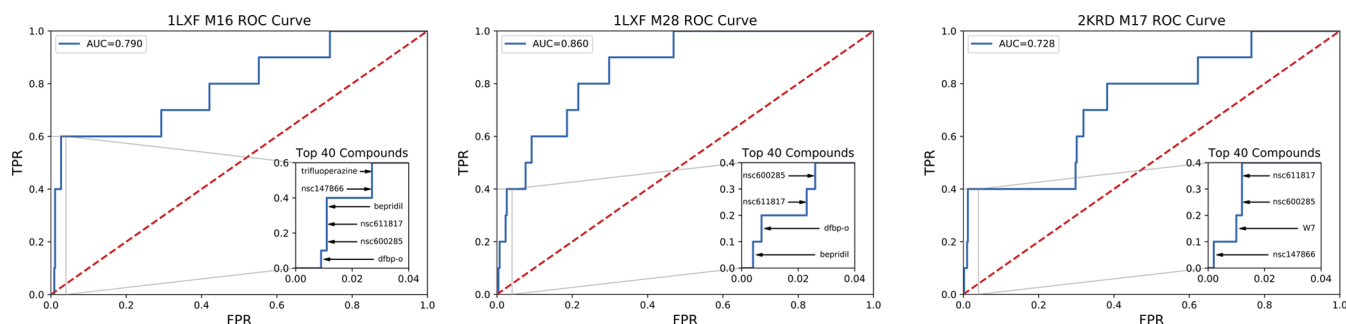


Figure 4. ROC curves depicting receptor conformer performance in active/decoy discrimination testing using Glide SP. The TPR is plotted against the FPR showing where the docking algorithm and conformer place the known active compounds with respect to the decoys. The graphic's zoomed inlay shows the top 40 docked compounds and highlights the true positives, along with their identities. The number of known cNTnC binders that ranked in the top 40 by the docking score was a key indicator for predictive receptor model selection.

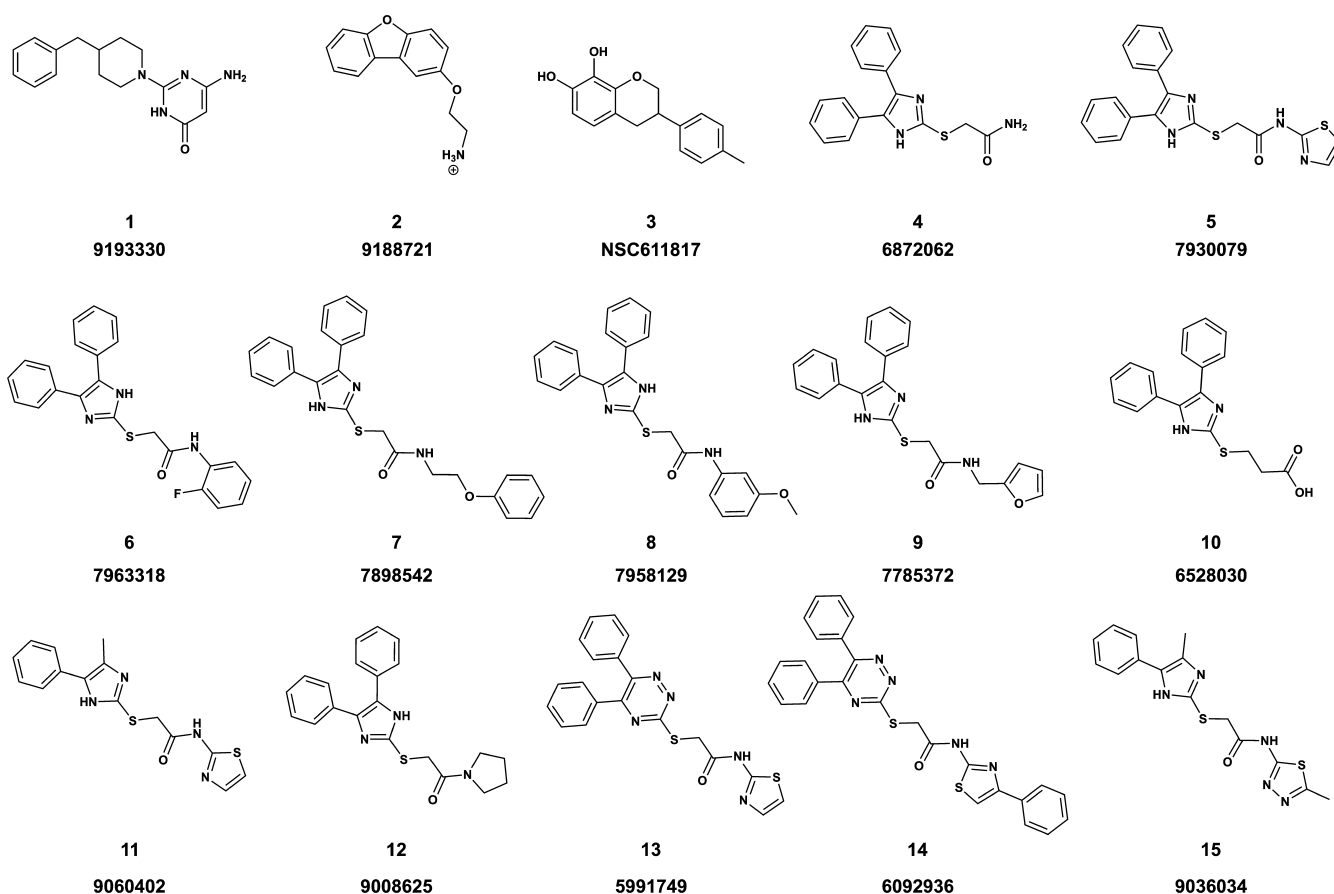


Figure 5. Experimental hits and highly similar compounds thereof along with their unique ChemBridge IDs below.

algorithm. These structures were preselected by filtering the Express Library based on $\log P$, MW, and the presence of PAINS functional groups. After the docking simulations we averaged the docking rank (based on the docking score) across all three receptor conformers. We hypothesized that active compounds would likely score well in all screened conformers. One drawback of targeting cNTnC's hydrophobic patch is that more nonpolar compounds tend to give higher docking scores because of the nonpolar environment of the binding site. However, for experimental assays it is critical that the compounds be soluble in aqueous buffer and, considering eventual druggability, high lipophilicity poses an additional hurdle. Thus, the top 45 compounds were filtered again according to $\log P$, this time using the Virtual Computational Chemistry Laboratory Web Service's ALOGPS 2.1 lipophilicity predictor. The postfilter removed five compounds from the top 40 because they fell above our 3.6 cutoff range. The next five ranked compounds meeting the $\log P$ cutoff criteria were substituted. The docked poses of the final 40 compounds were visually inspected to confirm docking into the hydrophobic patch of cNTnC and subsequently ordered from ChemBridge for *in vitro* assays.

Initial stopped-flow kinetics revealed that 30 of the initial 40 compounds were soluble enough in aqueous buffer that experimental measurements could be obtained. Of the 30 compounds that were able to be experimentally tested, 11 showed at least a 10% decrease of the Ca^{2+} dissociation rate for the chimera. The average Ca^{2+} dissociation rate observed for the chimera in the absence of compounds was $69.4 \pm 0.4 \text{ s}^{-1}$. Compounds 1 and 2 (Figure 5) led to a moderate slowing of

the Ca^{2+} dissociation rate to 49.1 ± 0.5 and $50.7 \pm 0.6 \text{ s}^{-1}$ at $100 \mu\text{M}$. These rates were similar to those observed with compounds that we previously discovered,³⁷ compound 3 ($52.9 \pm 0.4 \text{ s}^{-1}$) at $100 \mu\text{M}$. Compound 4 performed the best of the initial compounds screened, leading to a slowing in the Ca^{2+} dissociation rate to $32.6 \pm 0.5 \text{ s}^{-1}$ at $100 \mu\text{M}$.

To further characterize our top hit, compound 4 (whose bound pose can be seen in Figure 6), we carried out stopped-

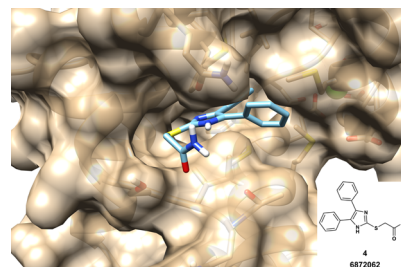


Figure 6. Bound pose of initial hit, compound 4, revealing lipophilic phenyl groups positioned back in the hydrophobic patch.

flow experiments using increasing concentrations of compound 4 in order to get a dose response. We also compared the effect of compound 4 on the rate of Ca^{2+} dissociation from the chimera to that of previously discovered compound 3. Our results, shown in Figure 7, panel A (with representative stopped-flow traces shown in Figure 7, panel B), indicate the ability of compound 4 to slow the rate of Ca^{2+} dissociation from chimera was greater than that of compound 3.

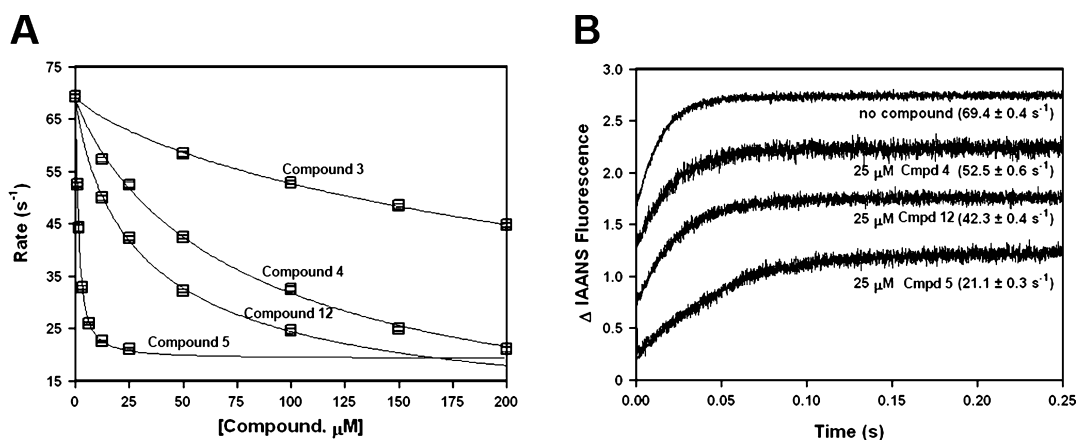


Figure 7. Effect of compounds on the rate of Ca²⁺ dissociation from the chimera. Panel (A) shows the plot of the apparent rates of Ca²⁺ dissociation from the chimera in the presence of increased concentrations of compounds 3, 4, 12, or 5. Each data point represents an average of at least three measurements \pm standard error. Data were fit with an asymmetric sigmoid curve. The half-maximal values were 430 ± 138 , 84 ± 30 , 34 ± 12 , and $1.45 \pm 0.09 \mu\text{M}$ for compounds 3, 4, 12, and 5, respectively. Panel (B) shows representative stopped-flow traces as Ca²⁺ is removed from the chimera in the presence or absence of 25 μM of compounds 4, 12, or 5. Rates of Ca²⁺ dissociation were measured following the fluorescence of IAANS attached to Cys⁵³ of the chimera with C35S, T53C, and C84S substitutions. In order to measure the rates of Ca²⁺ dissociation, the chimera (0.5 μM) in the absence or presence of compounds in the stopped-flow buffer (10 mM MOPS, 150 mM KCl, at pH 7.0) containing 200 μM Ca²⁺ was rapidly mixed with an equal volume of EGTA (10 mM) in the stopped-flow buffer, in the absence or presence of compounds. The traces have been normalized and staggered for clarity.

Compound 4 was determined to have an apparent experimental affinity of $84 \pm 30 \mu\text{M}$, while compound 3 was determined to have an apparent experimental affinity of $430 \pm 138 \mu\text{M}$. Thus, compound 4 displayed an \sim fivefold increase in apparent experimental affinity. The bound pose of compound 4 positions the lipophilic phenyl rings branching off of the imidazole core nestled deep within the hydrophobic patch while the more polar amido moiety positions itself to be more solvent exposed, potentially interacting favorably with cTnI. Encouraged by our initial success with compound 4 we closely analyzed the entirety of the ChemBridge EXPRESS-Pick Collection for compounds with similar scaffolds. We took a cheminformatics approach and utilized the RDKit package as implemented in Python 3.6 to fingerprint all 504,599 library compounds with the default, RDKit-specific fingerprint scheme and compared all fingerprints to compound 4 in order to identify structurally similar compounds. A similarity threshold of 0.70 was used as a cutoff. With this cut-off, 20 additional compounds were identified. Each compound was docked into the top performing receptor model, 1LXF M16, the compounds were ranked by docking score, and the top five were purchased for further experimental testing (compounds 5–9, Figure 5). An additional compound (10) that did not score as well in docking trials but still differed by only one functional group with respect to compound 4 was also purchased and tested. For compound 10, the terminal amide was substituted with a carboxylic acid (calculated Tanimoto similarity coefficients with respect to compound 4 available in Table S4).

Additional stopped-flow experiments revealed that three of these compounds performed relatively well. At 12.5 μM , compounds 8 and 9 slowed the calcium off-rate to 45.5 ± 0.4 and $47.5 \pm 0.4 \text{ s}^{-1}$, respectively. It was also the case that compound 5 (Figure 5) was able to slow the Ca²⁺ dissociation rate from the chimera by \sim 70% (to $21.1 \pm 0.3 \text{ s}^{-1}$ at 25 μM) (Figure 7). Not only was the Ca²⁺ dissociation rate in the presence of compound 5 significantly slower compared to compound 4 at 25 μM , the apparent binding affinity was

determined to be $1.45 \pm 0.09 \mu\text{M}$, placing compound 5 amongst the most potent and highest affinity cTnC-cTnI Ca²⁺ sensitivity modulators known to date. The seemingly simplistic modification of the terminal amide to include a thiazole ring was able to increase effective binding by over a factor of 10. The thiazolium containing compound 5 and the initial hit, compound 4, display similar bound poses where the hydrophobic phenyl groups attached to the core imidazole lie tightly situated in the hydrophobic patch. A view of compound 5's docked pose as well as an overlay of the docked poses for both compounds 4 and 5 can be seen in Figure 8. We observed a

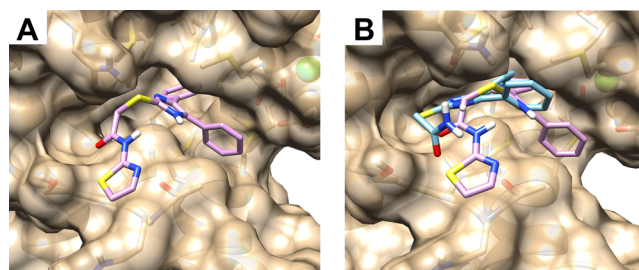


Figure 8. Bound pose of lead experimental hit (compound 5) obtained from docking simulation (panel A) and overlay of the two top performing compounds 4 and 5 (panel B).

moderate shift in the positioning of the 4,5-diphenyl imidazole core. It appears in the docked structure that one of the phenyl rings shifted deeper into the hydrophobic patch. This spatial rearrangement may occur to accommodate an alternate favorable positioning (compared to compound 4) of the terminal thiazolium ring. To verify that compounds 4 and 5 decreased the rate of Ca²⁺ dissociation from chimera by increasing Ca²⁺ sensitivity, we compared stopped-flow amplitudes measured at sub-saturating Ca²⁺ (1 μM) to amplitudes measured at saturating Ca²⁺ (200 μM) for chimera in the absence or presence of compounds 4 or 5. Figure 9 shows that presence of compounds 4 (at 50 μM) or 5 (at 12.5

μM) led to higher Ca^{2+} saturation of chimera at sub-saturating Ca^{2+} , indicative of higher Ca^{2+} sensitivity.

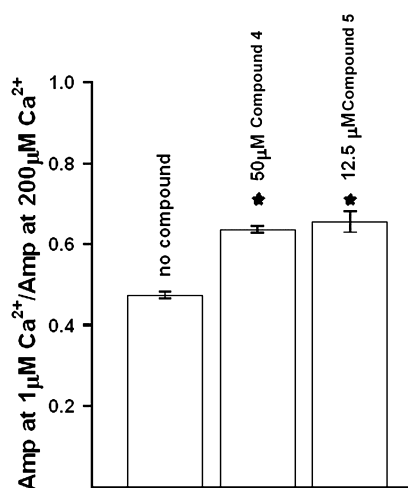


Figure 9. Ca^{2+} sensitizing effect of the compounds. The bar graphs show the effect of compounds 5 or 4 on the ratio of the amplitude of stopped-flow traces at 1 μM Ca^{2+} to the amplitude at 200 μM Ca^{2+} . To measure amplitudes at 1 μM Ca^{2+} , the chimera (0.5 μM) in the absence or presence of 12.5 μM of compound 5 or 50 μM of compound 4 in the stopped-flow buffer containing 1 μM Ca^{2+} was rapidly mixed with an equal volume of EGTA (10 mM) in the stopped-flow buffer, in the absence or presence of 12.5 μM of compound 5 or 50 μM of compound 4. To measure amplitudes at 200 μM Ca^{2+} , the chimera (0.5 μM) in the absence or presence of 12.5 μM of compound 5 or 50 μM of compound 4 in the stopped-flow buffer containing 200 μM Ca^{2+} was rapidly mixed with an equal volume of EGTA (10 mM) in the stopped-flow buffer, in the absence or presence of 12.5 μM of compound 5 or 50 μM of compound 4. Data represent the mean \pm standard error of at least three separate experiments.

We continued efforts in performing a preliminary SAR by locating purchasable compounds with similar structures and docking profiles to our known hits. Tanimoto similarity searches comparing compound 5 to the rest of the ChemBridge EXPRESS-Pick Collection (at a similarity cutoff of 0.7) revealed two additional unique compounds that had not been previously purchased or tested. Additionally, we lowered our similarity criteria to 0.55 in order to expand the list of new potential compounds to test. We then took a two-pronged approach where the 42 compounds identified with our less stringent similarity requirements were docked into the top performing receptor model 1LXF M16. Compounds with docking scores below the mean score were removed from consideration and ranked by similarity. In a second list the compounds were only ranked according to their similarity from most similar to least. By taking into account similarities, docking scores, and chemical intuition five additional compounds were selected for experimental screening. These compounds (compounds 11–15 in Figure 5) all had similarities greater than 0.60 when compared to compound 5 and encapsulated rather minor structural modifications to this newest lead compound (Tanimoto coefficients comparing these structures to compound 5 available in Table S5). Two particularly interesting compounds are described in detail below.

Compounds 11 and 12 (Figure 5) represent interesting cases in which a single functionality was changed from the lead

compound 5. In the case of compound 11, one of the lipophilic phenyl rings was exchanged for a methyl group. We reasoned that this compound should have diminished binding capabilities compared to compound 5 because one of the “anchoring” lipophilic phenyl rings had been replaced with a methyl group. While this aforementioned substitution could help with solubility, it would not be likely to increase binding ability or ability to slow Ca^{2+} dissociation rate. Experimentally this was the case; some binding and activity was retained, but in an extremely diminished capacity. Compound 12 provided another case to probe the effect of the terminal amide on binding and potency. Substitution of the thiazole-2-amine with a pyrrolidine ring showed improvement over the standard terminal amide, however, did not quite reach the binding affinity of compound 5 giving an approximate affinity of 34 ± 12 μM , determined by dose response experiments (Figure 7).

CONCLUSIONS

The goal of this study was twofold: (1) to see if the confidence in our screening process could be increased by vastly increasing the number of receptor structures screened as well as using self-docking to replicate experiment and (2) to add high-affinity compounds to the existing pool of cardiac troponin Ca^{2+} sensitizers. Importantly, we utilized a self-docking methodology in order to determine an optimal scoring function and set of parameters based on known experimental results. We then performed all of our virtual screening studies with these identified parameters. We screened a large number of receptor conformations (206 total) in order to increase the likelihood of discovering conformers able to correctly predict known cNTnC binders. The ChemBridge EXPRESS-Pick collection was prefiltered using a cheminformatics approach. The filtered library was screened against three predictive receptor conformers and the top 40 compounds were ordered for *in vitro* testing. Initial stopped-flow kinetics indicated that three of these compounds (1, 2, and 4) all appreciably slowed the dissociation rate of Ca^{2+} from the chimera, with compound 4 being the most potent by slowing the dissociation rate by $\sim 53\%$ with an affinity \sim fivefold greater than our previously reported compound 3.

Based on the initial encouraging experimental results a Tanimoto similarity search was performed (utilizing the RDKit-specific fingerprinting algorithm) focusing on lead compound 4. This iterative refinement led to the discovery and purchase of highly similar compound 5 with a Tanimoto coefficient of 0.75 as well as structurally similar and also active compounds 8 and 9. Compound 5 slowed the dissociation of Ca^{2+} by $\sim 70\%$ and it had an apparent binding affinity of 1.45 ± 0.09 μM (~ 300 -fold stronger than in our previous study) placing it among the most potent cNTnC binders and Ca^{2+} sensitivity modulators known to date. An additional Tanimoto search revealed a third highly similar compound to both 4 and 5 (compound 12); however this compound had experimental performance in-between compounds 4 and 5.

Compound 4 represents a novel pharmacophore as a cNTnC binder that shows proven potential for refined optimization realized by the increased efficacy from substitution of the terminal amide in compound 5. While the lipophilic phenyl groups situate themselves deep within the hydrophobic patch there are likely additional interactions between the head amine and other portions of the protein target. Future studies will focus on identifying and refining these interactions to increase compound performance and

specificity. As the number of known cNTnC Ca²⁺ sensitizers increases, it will only help to refine the computer-aided drug discovery process. Further high-throughput virtual screening and hit identification could potentially lead to quantitative structure–activity relationship modeling as well as hit-to-lead optimization with free energy methodologies.

The solubility of target compounds for screening still presented a significant barrier to the experimental study of these small molecules despite the usage of well-known log *P* predictors such as Wildman and Crippen's model as well as ALOGPS. While these log *P* models may have minimally mitigated the situation, many compounds still exhibited poor solubility particularly at high concentrations. Hopefully, by extending the knowledge base of experimental solubilities, especially focusing on attainable solution concentrations, modeling will be able to help guide selection of compounds amenable to *in vitro* testing in the future. The number of receptors studied with GaMD could be increased for even more structural variety. Additionally, alchemical calculations focused on the lead compound **5** could help elucidate key functionality that leads to binding or additionally provide routes to further fine-tune the strength of binding/calcium sensitization.

In conclusion, we have identified a number of novel compounds that slowed the Ca²⁺ dissociation from the chimera and had an overall Ca²⁺ sensitization effect. Notably, one of the compounds had an affinity for the chimera in the low micromolar range. These compounds were discovered through high-throughput virtual screening coupled with experimental verification. It is our hope that further refinement and testing will lead to the use Ca²⁺ sensitizers as therapeutics for heart failure in the near future.

■ ASSOCIATED CONTENT

SI Supporting Information

The Supporting Information is available free of charge at <https://pubs.acs.org/doi/10.1021/acs.jcim.0c00452>.

GaMD simulation details; receptor conformer numbers and sources; enrichment factors and AUCs; ordered compounds based on first Tanimoto similarity search; and ordered compounds based on second Tanimoto similarity search (PDF)

■ AUTHOR INFORMATION

Corresponding Author

Steffen Lindert – Department of Chemistry and Biochemistry, Ohio State University, Columbus, Ohio 43210, United States; orcid.org/0000-0002-3976-3473; Phone: 614-292-8284; Email: lindert.1@osu.edu; Fax: 614-292-1685

Authors

William H. Coldren – Department of Chemistry and Biochemistry, Ohio State University, Columbus, Ohio 43210, United States; orcid.org/0000-0003-2260-3809

Svetlana B. Tikunova – Davis Heart and Lung Research Institute and Department of Physiology and Cell Biology, Ohio State University, Columbus, Ohio 43210, United States

Jonathan P. Davis – Davis Heart and Lung Research Institute and Department of Physiology and Cell Biology, Ohio State University, Columbus, Ohio 43210, United States

Complete contact information is available at: <https://pubs.acs.org/doi/10.1021/acs.jcim.0c00452>

Author Contributions

§J.P.D. and S.L. are co-senior authors

Funding

Research reported in this publication was supported by the NHLBI institute of NIH under award numbers R01 HL137015 (to S.L.) and R01 HL132213 (to J.P.D.).

Notes

The authors declare no competing financial interest.

■ ACKNOWLEDGMENTS

The authors would like to thank the members of the Lindert group for useful discussions. We would like to thank the Ohio Supercomputer Center for valuable computational resources.⁶⁷

■ REFERENCES

- (1) Heron, M. *Deaths: Leading Causes for 2017*; National Center for Health Statistics: Hyattsville, MD, 2017; Vol. 68 (6).
- (2) *World Health Statistics 2018: Monitoring Health for the SDGs, Sustainable Development Goals*; World Health Organization: Geneva, 2018.
- (3) Mozaffarian, D.; Benjamin, E. J.; Go, A. S.; Arnett, D. K.; Blaha, M. J.; Cushman, M.; Das, S. R.; Ferranti, S. d.; Després, J.-P.; Fullerton, H. J.; Howard, V. J.; Huffman, M. D.; Isasi, C. R.; Jiménez, M. C.; Judd, S. E.; Kissela, B. M.; Lichtman, J. H.; Lisabeth, L. D.; Liu, S.; Mackey, R. H.; Magid, D. J.; McGuire, D. K.; Mohler, E. R.; Moy, C. S.; Muntner, P.; Mussolino, M. E.; Nasir, K.; Neumar, R. W.; Nichol, G.; Palaniappan, L.; Pandey, D. K.; Reeves, M. J.; Rodriguez, C. J.; Rosamond, W.; Sorlie, P. D.; Stein, J.; Towfighi, A.; Turan, T. N.; Virani, S. S.; Woo, D.; Yeh, R. W.; Turner, M. B. Heart Disease and Stroke Statistics—2016 Update. *Circulation* **2016**, *133*, 447–454.
- (4) Remme, W.; Swedberg, K. Guidelines for the Diagnosis and Treatment of Chronic Heart Failure. *Eur. Heart J.* **2001**, *22*, 1527–1560.
- (5) Yan, C.; Miller, C. L.; Abe, J.-i. Regulation of Phosphodiesterase 3 and Inducible cAMP Early Repressor in the Heart. *Circ. Res.* **2007**, *100*, 489–501.
- (6) Perrone, S. V.; Kaplinsky, E. J. Calcium Sensitizer Agents: A New Class of Inotropic Agents in the Treatment of Decompensated Heart Failure. *Int. J. Cardiol.* **2005**, *103*, 248–255.
- (7) Lee, J. A.; Allen, D. G. Calcium Sensitizers. *Br. Med. J.* **1990**, *300*, 551–552.
- (8) Solaro, R. J.; Rüegg, J. C. Stimulation of Ca⁺⁺ Binding and ATPase Activity of Dog Cardiac Myofibrils by AR-L 115BS, a Novel Cardiotonic Agent. *Circ. Res.* **1982**, *51*, 290–294.
- (9) Shettigar, V.; Zhang, B.; Little, S. C.; Salhi, H. E.; Hansen, B. J.; Li, N.; Zhang, J.; Roof, S. R.; Ho, H.-T.; Brunello, L.; Lerch, J. K.; Weisleder, N.; Fedorov, V. V.; Accornero, F.; Rafael-Fortney, J. A.; Gyorke, S.; Janssen, P. M. L.; Biesiadecki, B. J.; Ziolo, M. T.; Davis, J. P. Rationally Engineered Troponin C Modulates *in vivo* Cardiac Function and Performance in Health and Disease. *Nat. Commun.* **2016**, *7*, 10794.
- (10) *Novel Drug Approvals for 2018*|FDA; U.S. Food & Drug Administration: Silver Spring, MD, 2018.
- (11) Davis, J. P.; Tikunova, S. B. Ca²⁺ Exchange with Troponin C and Cardiac Muscle Dynamics. *Cardiovasc. Res.* **2007**, *77*, 619–626.
- (12) Davis, J. P.; Shettigar, V.; Tikunova, S. B.; Little, S. C.; Liu, B.; Siddiqui, J. K.; Janssen, P. M. L.; Ziolo, M. T.; Walton, S. D. Designing Proteins to Combat Disease: Cardiac Troponin C as an Example. *Arch. Biochem. Biophys.* **2016**, *601*, 4–10.
- (13) Carroll, R. G. Musculoskeletal System. In *Elsevier's Integrated Physiology*; Carroll, R. G., Ed.; Mosby: Philadelphia, 2007; pp 43–55.
- (14) Solaro, J.; Van Eyk, J. Altered Interactions Among Thin Filament Proteins Modulate Cardiac Function. *J. Mol. Cell. Cardiol.* **1996**, *28*, 217–230.
- (15) Li, M. X.; Wang, X.; Sykes, B. D. Structural Based Insights Into the Role of Troponin in Cardiac Muscle Pathophysiology. *J. Muscle Res. Cell Motil.* **2004**, *25*, 559–579.

- (16) Takeda, S.; Yamashita, A.; Maeda, K.; Maeda, Y. Structure of the Core Domain of Human Cardiac Troponin in the Ca^{2+} -Saturated Form. *Nature* **2003**, *424*, 35–41.
- (17) Perry, S. V. Troponin I: Inhibitor or facilitator. In *Muscle Physiology and Biochemistry*; Imai, S., Endo, M., Ohtsuki, I., Eds.; Springer, 1999; Vol. 31.
- (18) Gordon, A. M.; Regnier, M.; Homsher, E. Skeletal and Cardiac Muscle Contractile Activation: Tropomyosin “Rocks and Rolls”. *Physiology* **2001**, *16*, 49–55.
- (19) Siddiqui, J. K.; Tikunova, S. B.; Walton, S. D.; Liu, B.; Meyer, M.; de Tombe, P. P.; Neilson, N.; Keken-Huskey, P. M.; Salhi, H. E.; Janssen, P. M. L.; Biesiadecki, B. J.; Davis, J. P. Myofilament Calcium Sensitivity: Consequences of the Effective Concentration of Troponin I. *Front. Physiol.* **2016**, *7*, 632.
- (20) Lindert, S.; Keken-Huskey, P. M.; McCammon, J. A. Long-Timescale Molecular Dynamics Simulations Elucidate the Dynamics and Kinetics of Exposure of the Hydrophobic Patch in Troponin C. *Biophys. J.* **2012**, *103*, 1784–1789.
- (21) Bowman, J. D.; Lindert, S. Computational Studies of Cardiac and Skeletal Troponin. *Front. Mol. Biosci.* **2019**, *6*, 68.
- (22) Lindert, S.; Keken-Huskey, P. M.; Huber, G.; Pierce, L.; McCammon, J. A. Dynamics and Calcium Association to the N-Terminal Regulatory Domain of Human Cardiac Troponin C: A Multiscale Computational Study. *J. Phys. Chem. B* **2012**, *116*, 8449–8459.
- (23) Dewan, S.; McCabe, K. J.; Regnier, M.; McCulloch, A. D.; Lindert, S. Molecular Effects of ϵ TnC DCM Mutations on Calcium Sensitivity and Myofilament Activation—An Integrated Multiscale Modeling Study. *J. Phys. Chem. B* **2016**, *120*, 8264–8275.
- (24) Bowman, J. D.; Lindert, S. Molecular Dynamics and Umbrella Sampling Simulations Elucidate Differences in Troponin C Isoform and Mutant Hydrophobic Patch Exposure. *J. Phys. Chem. B* **2018**, *122*, 7874–7883.
- (25) Bowman, J. D.; Coldren, W. H.; Lindert, S. Mechanism of Cardiac Troponin C Calcium Sensitivity Modulation by Small Molecules Illuminated by Umbrella Sampling Simulations. *J. Chem. Inf. Model.* **2019**, *59*, 2964–2972.
- (26) Haikala, H.; Kaivola, J.; Nissinen, E.; Wall, P. I.; Levijoki, J.; Lindén, I.-B. Cardiac Troponin C as a Target Protein for a Novel Calcium Sensitizing Drug, Levosimendan. *J. Mol. Cell. Cardiol.* **1995**, *27*, 1859–1866.
- (27) Nieminen, M. S.; Fruhwald, S.; Heunks, L. M.; Suominen, P. K.; Gordon, A. C.; Kivikko, M.; Pollesello, P. Levosimendan: Current Data, Clinical Use and Future Development. *Heart Lung Vessel* **2013**, *5*, 227–245.
- (28) Pollesello, P.; Ovaska, M.; Kaivola, J.; Tilgmann, C.; Lundström, K.; Kalkkinen, N.; Ulmanen, I.; Nissinen, E.; Taskinen, J. Binding of a New Ca^{2+} Sensitizer, Levosimendan, to Recombinant Human Cardiac Troponin C. *J. Biol. Chem.* **1994**, *269*, 28584–28590.
- (29) Pineda-Sanabria, S. E.; Robertson, I. M.; Sun, Y.-B.; Irving, M.; Sykes, B. D. Probing the Mechanism of Cardiovascular Drugs Using a Covalent Levosimendan Analog. *J. Mol. Cell. Cardiol.* **2016**, *92*, 174–184.
- (30) Solaro, R. J.; Bousquet, P.; Johnson, J. D. Stimulation of Cardiac Myofilament Force, ATPase Activity and Troponin C Ca^{2+} Binding by Bepridil. *J. Pharmacol. Exp. Ther.* **1986**, *238*, 502–507.
- (31) Varughese, J. F.; Baxley, T.; Chalovich, J. M.; Li, Y. A Computational and Experimental Approach To Investigate Bepridil Binding with Cardiac Troponin. *J. Phys. Chem. B* **2011**, *115*, 2392–2400.
- (32) Lindert, S.; Li, M. X.; Sykes, B. D.; McCammon, J. A. Computer-Aided Drug Discovery Approach Finds Calcium Sensitizer of Cardiac Troponin. *Chem. Biol. Drug Des.* **2015**, *85*, 99–106.
- (33) Cai, F.; Li, M. X.; Pineda-Sanabria, S. E.; Geloza, S.; Lindert, S.; West, F.; Sykes, B. D.; Hwang, P. M. Structures Reveal Details of Small Molecule Binding to Cardiac Troponin. *J. Mol. Cell. Cardiol.* **2016**, *101*, 134–144.
- (34) Nagy, L.; Pollesello, P.; Haikala, H.; Végh, Á.; Sorsa, T.; Levijoki, J.; Szilágyi, S.; Edes, I.; Tóth, A.; Papp, Z.; Papp, J. G. ORM-3819 Promotes Cardiac Contractility Through Ca^{2+} Sensitization in Combination with Selective PDE III Inhibition, a Novel Approach to Inotropy. *Eur. J. Pharmacol.* **2016**, *775*, 120–129.
- (35) Tikunova, S. B.; Cuesta, A.; Price, M.; Li, M. X.; Belevych, N.; Biesiadecki, B. J.; Reiser, P. J.; Hwang, P. M.; Davis, J. P. 3-chlorodiphenylamine Activates Cardiac Troponin by a Mechanism Distinct From Bepridil or TFP. *J. Gen. Physiol.* **2018**, *151*, 9–17.
- (36) Sugawara, H.; Endoh, M. A Novel Cardiotonic Agent SCH00013 Acts as a Ca^{++} Sensitizer with No Chronotropic Activity in Mammalian Cardiac Muscle. *J. Pharmacol. Exp. Ther.* **1998**, *287*, 214–222.
- (37) Aprahamian, M. L.; Tikunova, S. B.; Price, M. V.; Cuesta, A. F.; Davis, J. P.; Lindert, S. Successful Identification of Cardiac Troponin Calcium Sensitizers Using a Combination of Virtual Screening and ROC Analysis of Known Troponin C Binders. *J. Chem. Inf. Model.* **2017**, *57*, 3056–3069.
- (38) Lin, J.-H.; Perryman, A. L.; Schames, J. R.; McCammon, J. A. Computational Drug Design Accommodating Receptor Flexibility: The Relaxed Complex Scheme. *J. Am. Chem. Soc.* **2002**, *124*, 5632–5633.
- (39) Lin, J.-H.; Perryman, A. L.; Schames, J. R.; McCammon, J. A. The Relaxed Complex Method: Accommodating Receptor Flexibility for Drug Design with an Improved Scoring Scheme. *Biopolymers* **2003**, *68*, 47–62.
- (40) Amaro, R. E.; Baron, R.; McCammon, J. A. An Improved Relaxed Complex Scheme for Receptor Flexibility in Computer-aided Drug Design. *J. Comput.-Aided Mol. Des.* **2008**, *22*, 693–705.
- (41) Li, M. X.; Robertson, I. M.; Sykes, B. D. Interaction of Cardiac Troponin with Cardiotonic Drugs: A Structural Perspective. *Biochem. Biophys. Res. Commun.* **2008**, *369*, 88–99.
- (42) Oleszczuk, M.; Robertson, I. M.; Li, M. X.; Sykes, B. D. Solution Structure of the Regulatory Domain of Human Cardiac Troponin C in Complex with the Switch Region of Cardiac Troponin I and W7: The Basis of W7 as an Inhibitor of Cardiac Muscle Contraction. *J. Mol. Cell. Cardiol.* **2010**, *48*, 925–933.
- (43) Hoffman, R. M. B.; Sykes, B. D. Structure of the Inhibitor W7 Bound to the Regulatory Domain of Cardiac Troponin C. *Biochemistry* **2009**, *48*, 5541–5552.
- (44) Cai, F.; Hwang, P. M.; Sykes, B. D. Structural Changes Induced by the Binding of the Calcium Desensitizer W7 to Cardiac Troponin. *Biochemistry* **2018**, *57*, 6461–6469.
- (45) Wang, X.; Li, M. X.; Sykes, B. D. Structure of the Regulatory N-domain of Human Cardiac Troponin C in Complex with Human Cardiac Troponin I₁₄₇₋₁₆₃ and Bepridil. *J. Biol. Chem.* **2002**, *277*, 31124–31133.
- (46) Case, D. A.; Ben-Shalom, I. Y.; Brozell, S. R.; Cerutti, D. S.; Cheatham, T. E. I.; Cruzeiro, V. W. D.; Darden, T. A.; Duke, R. E.; Ghoreishi, D.; Gilson, M. K.; Gohlke, H.; Goetz, A. W.; Greene, D.; Harris, R.; Homeyer, N.; Izadi, S.; Kovalenko, A.; Kurtzman, T.; Lee, T. S.; LeGrand, S.; Li, P.; Lin, C.; Lieu, J.; Luchko, T.; Luo, R.; Mermelstein, D. J.; Merz, K. M.; Miao, Y.; Monard, G.; Nguyen, C.; Nguyen, H.; Omelyan, I.; Onufriev, A.; Pan, F.; Qi, R.; Roe, D. R.; Roitberg, A.; Sagui, C.; Schott-Verdugo, S.; Shen, J.; Simmerling, C. L.; Smith, J.; Salomon-Ferrer, R.; Swails, J.; Walker, R. C.; Wang, J.; Wei, H.; Wolf, R. M.; Wu, X.; Xiao, L.; York, D. M.; Kollman, P. A. *AMBER 2018*; University of California: San Francisco: 2018.
- (47) Maier, J. A.; Martinez, C.; Kasavajhala, K.; Wickstrom, L.; Hauser, K. E.; Simmerling, C. ff14SB: Improving the Accuracy of Protein Side Chain and Backbone Parameters from ff99SB. *J. Chem. Theory Comput.* **2015**, *11*, 3696–3713.
- (48) Miao, Y.; Feher, V. A.; McCammon, J. A. Gaussian Accelerated Molecular Dynamics: Unconstrained Enhanced Sampling and Free Energy Calculation. *J. Chem. Theory Comput.* **2015**, *11*, 3584–3595.
- (49) Li, M. X.; Spyropoulos, L.; Sykes, B. D. Binding of Cardiac Troponin-I147-163 Induces a Structural Opening in Human Cardiac Troponin-C. *Biochemistry* **1999**, *38*, 8289–8298.

(50) Sastry, G. M.; Adzhigirey, M.; Day, T.; Annabhimoju, R.; Sherman, W. Protein and Ligand Preparation: Parameters, Protocols, and Influence on Virtual Screening Enrichments. *J. Comput.-Aided Mol. Des.* **2013**, *27*, 221–234.

(51) *Schrödinger Maestro, Release 2018-3*; Schrödinger: New York, NY, 2018.

(52) Shelley, J. C.; Cholleti, A.; Frye, L. L.; Greenwood, J. R.; Timlin, M. R.; Uchimaya, M. Epik: A Software Program for pKa Prediction and Protonation State Generation for Drug-like Molecules. *J. Comput.-Aided Mol. Des.* **2007**, *21*, 681–691.

(53) *Schrödinger Ligprep, Release 2018-3*; Schrödinger: New York, NY, 2018.

(54) Pentti, N.; Erkki, K.; Reigjo, B.; Tom, W.; Heimo, H.; Jorma, H. Preparation of (-)-[[4-(1,4,5,7-tetrahydro-4-methyl-6-oxo-3-pyridazinyl)pehnyl]hydrazono]propanedinitrile as a cardiotoxic agent, US patent US4946842A, 1992.

(55) Trott, O.; Olson, A. J. AutoDock Vina: Improving the Speed and Accuracy of Docking with a New Scoring Function, Efficient Optimization, and Multithreading. *J. Comput. Chem.* **2010**, *31*, 455–461.

(56) Forli, S.; Huey, R.; Pique, M. E.; Sanner, M. F.; Goodsell, D. S.; Olson, A. J. Computational Protein-ligand Docking and Virtual Drug Screening with the AutoDock suite. *Nat. Protoc.* **2016**, *11*, 905–919.

(57) Wang, R.; Lai, L.; Wang, S. Further Development and Validation of Empirical Scoring Functions for Structure-based Binding Affinity Prediction. *J. Comput.-Aided Mol. Des.* **2002**, *16*, 11–26.

(58) Friesner, R. A.; Banks, J. L.; Murphy, R. B.; Halgren, T. A.; Klicic, J. J.; Mainz, D. T.; Repasky, M. P.; Knoll, E. H.; Shelley, M.; Perry, J. K.; Shaw, D. E.; Francis, P.; Shenkin, P. S. Glide: A New Approach for Rapid, Accurate Docking and Scoring. 1. Method and Assessment of Docking Accuracy. *J. Med. Chem.* **2004**, *47*, 1739–1749.

(59) Friesner, R. A.; Murphy, R. B.; Repasky, M. P.; Frye, L. L.; Greenwood, J. R.; Halgren, T. A.; Sanschagrin, P. C.; Mainz, D. T. Extra Precision Glide: Docking and Scoring Incorporating a Model of Hydrophobic Enclosure for Protein–Ligand Complexes. *J. Med. Chem.* **2006**, *49*, 6177–6196.

(60) Halgren, T. A.; Murphy, R. B.; Friesner, R. A.; Beard, H. S.; Frye, L. L.; Pollard, W. T.; Banks, J. L. Glide: A New Approach for Rapid, Accurate Docking and Scoring. 2. Enrichment Factors in Database Screening. *J. Med. Chem.* **2004**, *47*, 1750–1759.

(61) Harder, E.; Damm, W.; Maple, J.; Wu, C.; Reboul, M.; Xiang, J. Y.; Wang, L.; Lupyan, D.; Dahlgren, M. K.; Knight, J. L.; Kaus, J. W.; Cerutti, D. S.; Krilov, G.; Jorgensen, W. L.; Abel, R.; Friesner, R. A. OPLS3: A Force Field Providing Broad Coverage of Drug-like Small Molecules and Proteins. *J. Chem. Theory Comput.* **2016**, *12*, 281–296.

(62) Pedregosa, F.; Varoquaux, G.; Gramfort, A.; Michel, V.; Thirion, B.; Grisel, O.; Blondel, M.; Prettenhofer, P.; Weiss, R.; Dubourg, V.; Vanderplas, J.; Passos, A.; Cournapeau, D.; Brucher, M.; Perrot, M.; Duchesnay, E. Scikit-learn: Machine Learning in Python. *J. Mach. Learn. Res.* **2011**, *12*, 2825–2830.

(63) Baell, J. B.; Holloway, G. A. New Substructure Filters for Removal of Pan Assay Interference Compounds (PAINS) from Screening Libraries and for Their Exclusion in Bioassays. *J. Med. Chem.* **2010**, *53*, 2719–2740.

(64) RDKit: *Open-Source Cheminformatics*, March 01, 2020; <http://www.rdkit.org>, accessed October 20, 2019.

(65) Wildman, S. A.; Crippen, G. M. Prediction of Physicochemical Parameters by Atomic Contributions. *J. Chem. Inf. Comput. Sci.* **1999**, *39*, 868–873.

(66) Davis, J. P.; Norman, C.; Kobayashi, T.; Solaro, R. J.; Swartz, D. R.; Tikunova, S. B. Effects of Thin and Thick Filament Proteins on Calcium Binding and Exchange with Cardiac Troponin C. *Biophys. J.* **2007**, *92*, 3195–3206.

(67) Ohio Supercomputer Center. *Ohio Technology Consortium of the Ohio Board of Regents*, 1987.